



1 Tracking Ionospheric Changes during Solar Eclipses: Concepción

2 Historical Data

- 3 Adán Y. Godoy¹, Manuel A. Bravo¹, Benjamín A. Urra¹, Carlos A. Castillo-Rivera², Marayén R.
- 4 Canales³, Alberto J. Foppiano¹
- ⁵ Centro de Instrumentación Científica, Universidad Adventista de Chile, Chillán, Ñuble, Chile
- 6 ²Departamento de Física, Universidad de Santiago de Chile, Estación Central, Santiago, Chile
- 7 ³Departamento de Geofísica, Universidad de Concepción, Concepción, Bío Bío, Chile
- 8 Correspondence to: Manuel A. Bravo (manuelbravo@unach.cl)
- 9 Abstract. Solar eclipses offer a unique natural experiment to probe ionospheric responses to sudden reductions in solar
- 10 radiation. This study examines the Concepción (36.79°S, 73.03°W/Chillán (36.64°S, 71.99°W) ionosphere during 16
- 11 selected eclipses, out of 21 identified events between 1958 and 2024, using a historical ionogram dataset spanning several
- 12 decades. Critical frequencies (foE, foF1, foF2) and virtual heights (h'E, h'F1, h'F2/F) were extracted from digitized and
- 13 scaled ionograms to quantify eclipse-induced perturbations. Diurnal variations show typical dips in the E- and F1-layer
- 14 critical frequencies, while F2-layer responses are more complex and variable. Regression analysis was performed
- 15 exclusively on critical frequencies, revealing a nearly linear decrease of foE with increasing solar obscuration, whereas
- 16 virtual heights exhibited inconsistent behavior due to neutral winds, plasma transport, and other dynamical processes.
- 17 High-cadence observations, available for select events, provided further insight into short-term ionospheric variability. Only
- 18 the 2 July 2019 and 14 December 2020 eclipse responses were previously published. The study highlights the rescue and
- 19 standardization of historical ionograms, many originally on fragile or hazardous 35 mm film, emphasizing the scientific
- 20 value of long-term datasets. Predictions for the 06 February 2027 eclipse indicate an expected foE decrease of ~0.7 MHz at
- 21 Chillán, offering a timely opportunity to validate the regression models and assess predictive skill across solar cycle
- 22 conditions.

23 1 Introduction

- 24 Solar eclipses offer unique opportunities to understand how the ionosphere reacts when solar radiation is interrupted during
- 25 daylight conditions. A "small night' generated by a total solar eclipse produces disturbances in the ionosphere, both directly
- 26 by the suppression of incident radiation or induced by chemical and transport processes. As solar radiation decreases, the
- 27 electron concentration of the ionospheric layers E and F1, which mainly depend on the production and loss terms, decrease
- 28 considerably or even disappear throughout the eclipse. Other layers, such as the F2 layer, for which the electron





29 concentration depends significantly on plasma transport by neutral winds and electrodynamics, react with delays and are

30 difficult to predict (Le et al., 2009; Hoque et al., 2016; Zhang et al., 2024). Furthermore, the ionosphere's response depends

31 on regional conditions and external factors such as space weather and lower atmospheric coupling. Additionally, changes in

32 the virtual and real heights of ionospheric layers, such as h'F1, h'F2/F, and hmF2, have been frequently reported, generally

33 showing an upward motion followed by a post-maximum descent as the ionosphere recovers (Le et al., 2008; Chuo, 2013;

34 Zhang et al., 2024).

35 Historically, from 1920 onward, studies of solar eclipses have progressively revealed how reduced solar radiation affects the

36 ionosphere (Ratcliffe, 1956). Early radio observations established solar radiation as the main ionization source and

37 highlighted layer-specific density and plasma transport effects. From 1960–2015, hundreds of studies based on observations

38 with instruments such as VLF receivers, GNSS arrays, ionosondes, riometers, incoherent scatter radars and Doppler systems

39 have determined eclipse-induced variations in TEC, foF2, hmF2, electron temperature, and ion velocities, etc. These studies

40 have consistently shown that during eclipses there are delayed responses, latitude-dependent effects, and evidence of

41 acoustic gravity waves (AGW) and traveling ionospheric disturbances. Major events like the 2017 Great American Eclipse

42 provided unprecedented high-resolution data, allowing detailed modeling and confirmation of earlier findings, while recent

43 studies emphasize the role of geomagnetic activity and AGW generation in modulating post-eclipse ionospheric dynamics.

44 A detailed review of these studies is compiled in Appendix A of Bravo et al. (2020).

45 Early days determination of ionospheric responses during solar eclipses was made mainly from ionosonde (vertically

46 incidence HF radar) observations. There are long time series of these observations, allowing the study of ionospheric

47 long-term trends. Early works are, for example, those of Smith and King, 1981; Bremer, 1992; Ortiz de Adler et al., 1997;

48 Jarvis et al., 1998; Foppiano et al., 1999. Later work has been reviewed by Lastovicka et al. (2017, and references within)

49 and recent progress reported by Lastovicka (2023). One of these long-term series also offers a unique dataset to analyze both

50 short-term eclipse-induced ionospheric variations and broader temporal trends in the South American sector (Bravo et al.,

51 2020).

52 The purpose of this work is to characterize the response of the Concepción (36.79°S, 73.03°W) ionosphere under solar

53 eclipse conditions over several solar cycles, so that its response can be associated with parameters such as the amount of

54 darkness, season, time of day, etc., in order to predict the response for future eclipses.

55 2 Methodology

56 2.1 Eclipse Event Selection and Station Characteristics

57 A comprehensive search was conducted to identify all solar eclipse events whose trajectory passed over the ionospheric

58 observation stations in central Chile during the period 1957–2024.





59 Ionospheric characteristics during these events were selected from the long series of ionosonde records (ionogram) of 60 ionospheric station j3o: Concepción (36.79°S, 73.03°W). The Concepción ionosonde was a C4 type (1-25 MHz range) and 61 associated antennae (crossed deltas), installed in 1957 at the Universidad de Concepción, Andalien campus, by personnel 62 from the National Bureau of Standards (NBS, USA) for the International Geophysical Year (Ramírez, 1963). Later, the 63 ionosonde was moved to the nearby Bellavista campus (less than 2 km), the sweep range modified (0.25-20 MHz) and the 64 antennae improved to make better use of the quiet electromagnetic environment (adjustable folded dipole 0.25 to 3 MHz and 65 log-periodic 3 to 20 MHz). Maintenance difficulties of the antennae lead to a change during 1975 (cross deltas again). The 66 C4 ionosonde operated till 1994 with a transmitted power of approximately 1-5 kW, and employed simple pulse 67 transmissions without signal coding. Ionograms were recorded on 35 mm film. The interpretation and scaling required 68 optical projection on a screen and visual determination of parameters using a manual overlay. The j3o station resumed 69 operation in 1999. An IPS 42 type ionosonde (1- 22 MHz) was installed using the existing antennae. Recording was 70 changed from photographic to digital and routine observations were made until 2012, when it was relocated approximately 71 100 km northeast to Chillán (36.64°S, 71.99°W), renamed as j3p, as part of an instrumentation modernization program 72 (Ovalle et al., 2017). For a short time interval a Canadian Advanced Digital Ionosonde (CADI) was also used. The 73 ionosondes were operated by dedicated academics, supported by electronic engineers and technicians (Muzzioli, 1977; 74 Bravo et al., 2011), providing continuous and high-quality measurements of ionospheric parameters (critical frequencies, 75 virtual heights, etc.). The ionosonde and antennae changes do not preclude standard accuracy of critical frequencies and 76 virtual heights since these parameters are not very system gain sensitive. Both locations share similar geomagnetic latitude 77 characteristics, enabling the construction of a long-term ionospheric database representative of the mid-latitude South 78 American sector.

79 From the initial catalog of eclipse events identified, we selected those with solar obscuration exceeding 15% as observed 80 from the station coordinates (21 events). This threshold was established to ensure detectable ionospheric perturbations while 81 maintaining sufficient statistical samples for comparative analysis. The selected events span various phases of the solar 82 cycle and include eclipses with obscuration levels ranging from partial to near-totality, providing a diverse dataset for 83 investigating the relationship between eclipse magnitude and ionospheric response.

84 2.2 Historical Ionogram Database

85 The ionospheric observations analyzed in this study comprise a unique historical archive of vertical incidence ionograms 86 recorded between 1958 and 2024. The sounding cadence varied throughout the operational period, with temporal resolutions 87 of 1 hour, 30 minutes, 15 minutes, 5 minutes and 1 minute, depending on the scientific objectives and operational 88 constraints of each campaign period. Higher-cadence observations (1–5 minute intervals) were typically implemented 89 during special events, including eclipse campaigns and geomagnetic storm monitoring periods.





- 90 The archival records consist primarily of 35 mm photographic film containing ionogram traces acquired by the C4
- 91 ionosonde (1957–1994, the IPS-42 system delivered digital ionograms during an intermediate period (1999-2012), the
- 92 CADI for a few days only, and the IPS 42 after that. A substantial portion of this historical dataset had not been previously
- 93 interpreted and scaled or had undergone only partial manual scaling, representing a significant untapped scientific resource
- 94 for long-term ionospheric studies.

95 2.3 Data Processing Pipeline

- 96 2.3.1 Digitization: SOCIO Software
- 97 Ionograms preserved on celluloid film were digitized using an Epson Perfection V600 Photo scanner at 1200 dpi resolution
- 98 to ensure adequate capture of trace details and frequency-height grid specifications. The digitized images required geometric
- 99 correction due to perspective distortion, film degradation, and variations in original recording formats across different
- 100 ionosonde systems.
- 101 To address these challenges, we developed the Software de Corrección de Ionogramas (SoCIo), a MATLAB-based tool
- 102 specifically designed for the geometric correction and standardization of historical ionogram imagery. SoCIo performs
- 103 automated detection of the frequency-height grid structure, applies perspective correction algorithms to compensate for
- 104 scanning distortions, and standardizes image dimensions according to the specific ionosonde system (C4, IPS-42, or CADI)
- 105 that generated each record. The software includes modules for handling common film deterioration artifacts, including
- 106 opaque regions, physical damage, and inconsistent image density. This preprocessing step was essential for ensuring
- 107 accurate subsequent parameter extraction, as uncorrected geometric distortions can introduce systematic errors in frequency
- 108 and height measurements.
- 109 2.3.2 Scaling: DISS Software Enhancement
- 110 Following geometric correction, ionospheric parameters were extracted using the Digitized Ionogram Scaling Software
- 111 (DISS v. 3.0), previously employed in eclipse observation campaigns (Bravo et al., 2020). For the present study, DISS
- 112 capabilities were substantially enhanced to accommodate the diversity and technical challenges of the historical dataset. Key
- 113 improvements included: (1) implementation of interactive trace digitization tools enabling manual extraction of
- 114 frequency-virtual height coordinates from user-drawn traces on the ionogram display, (2) development of selectable
- 115 region-of-interest functionality to isolate specific ionospheric layers for detailed analysis, (3) incorporation of adjustable
- 116 frequency and height calibration parameters to fine-tune the pixel-to-physical-unit conversion for each ionogram variant,
- 117 and (4) integration of quality control modules to identify and flag problematic traces requiring manual review.
- 118 These enhancements enabled DISS to handle the heterogeneous characteristics of multi-decade ionosonde observations,
- 119 including variations in frequency sweep ranges (typically 1–20 MHz with system-dependent upper limits), height display





- 120 scales (100–500 km, later extended to 1000 km for topside observations), and trace characteristics influenced by film aging 121 and storage conditions.
- 122 2.3.3 Parameter Extraction
- 123 From each scaled ionogram, we extracted the following standard ionospheric parameters: critical frequencies of the E, F1,
- 124 and F2 layers (foE, foF1, foF2) and their corresponding virtual heights (h'E, h'F1, h'F2/F).

125 2.4 Statistical Analysis and Eclipse Response Quantification

- 126 Eclipse-induced ionospheric perturbations were quantified by calculating both absolute and percentage deviations of critical
- 127 frequencies relative to reference day median values at corresponding local times. Absolute deviations were computed as:

$$\Delta foL = foL_{eclinse} - foL_{reference}$$

129 where L represents the ionospheric layer (E, F1, F2). Percentage deviations were calculated as:

$$\% \Delta foL = \frac{foL_{eclipse} - foL_{reference}}{foL_{reference}} \times 100$$

- 131 Reference day values were obtained from monthly median parameters of each eclipse event, selecting the median value
- 132 across multiple reference days to minimize day-to-day ionospheric variability. When multiple measurements were available
- 133 during the eclipse period (depending on the operational cadence: 1, 5, 15, 30, or 60 minutes), we selected the observation
- 134 closest to the time of maximum obscuration for regression analysis.
- 135 Linear regression analysis was performed using NumPy's polyfit function (NumPy v1.24.0) to investigate the functional
- 136 relationship between solar obscuration percentage (independent variable, x) and ionospheric parameter deviations
- 137 (dependent variable, y). The regression model adopted was:

$$y = mx + b$$

139 where m represents the sensitivity of the ionospheric parameter to eclipse magnitude (slope) and b the intercept. The

140 goodness of fit was assessed using the coefficient of determination (r^2), computed as:

141
$$r^{2} = 1 - \frac{\sum_{i=1}^{n} (y_{i} - \widehat{y_{i}})^{2}}{\sum_{i=1}^{n} (y_{i} - \widehat{y})^{2}}$$







142 where y_i are observed values, $\hat{y_i}$ are predicted values from the regression line, and \bar{y} is the mean of observed values. r^2 quantifies the proportion of variance in ionospheric response explained by solar obscuration, with values ranging from 0 (no

144 explanatory power) to 1 (perfect prediction).

145 From the initial catalog of 21 eclipse events identified over the period 1957–2024 (see Table 1), we selected events 146 exhibiting clear ionospheric signatures and sufficient data coverage during the eclipse period. Both absolute (MHz) and 147 percentage (%) deviations were analyzed to assess whether normalization by baseline values improved the linearity of the 148 eclipse response. The heterogeneous nature of the dataset—comprising observations from three different ionosonde systems 149 (C4, IPS-42, CADI) with varying temporal resolutions—introduces additional variability that may affect correlation 150 strength, particularly for parameters sensitive to instrumental characteristics.

151 Table 1: Timing of selected solar eclipses over Concepción/Chillán (Maximum darkness >15%) from 1958 to 2030, 152 including start, maximum, and end times, according to Eclipse Calculator 2.0 (Masana, 2012).

| # | Date (DD-MM-YYYY) | Start time in Concepción (hh:mm UT) | Maximum time in Concepción (hh:mm UT) | End time in Concepción (hh:mm UT) | Maximum darkness in Concepción/ Chillán (%) | Ionospheric Station: j3o, Concepción; j3p, Chillán | Eclipse-time sampling interval |
|----|----------------------|---|---|---|--|--|--------------------------------------|
| 1 | 12-10-1958 | 21:32 | 22:31 | 23:01 | 95 | j3o: C4, cross deltas, 1-25 MHz | 5 min film |
| 2 | 25-01-1963 | 11:02 | 12:04 | 13:14 | 73 | j3o: C4, cross deltas, 1-25 MHz | 1 hour film |
| 3 | 12-11-1966 | 12:46 | 13:51 | 15:00 | 49 | j3o: C4, folded dipole + logperiodic, 0.25-20 MHz | 5 min film |
| 4 | 11-09-1969 | 21:03 | 21:53 | 22:35 | 20 | j3o: C4, folded dipole + logperiodic, 0.25-20 MHz | 30 min film |
| 5 | 04-01-1973 | 13:14 | 14:50 | 16:39 | 78 | j3o: C4, folded dipole + logperiodic, 0.25-20 MHz | 5 min film |
| 6 | 03-11-1975 | 11:22 | 12:06 | 12:52 | 19 | ј30 | Instrument failure |
| 7 | 22-08-1979 | 16:35 | 18:04 | 19:27 | 31 | j3o: C4, cross deltas, 0.25-20 MHz | 30 min film |
| 8 | 10-08-1980 | 19:47 | 20:51 | 21:49 | 27 | j3o: C4, cross deltas, 0.25-20 MHz | No data |
| 9 | 04-02-1981 | 22:25 | 23:18 | 23:56 | 43 | j3o: C4, cross deltas, 0.25-20 MHz | 1 hour film |
| 10 | 12-11-1985 | 12:36 | 13:20 | 14:06 | 17 | j3o: C4, cross deltas, 0.25-20 MHz | 1 hour film |
| 11 | 29-03-1987 | 11:07 | 11:07 | 12:01 | 58 | j3o: C4, cross deltas, | 1 hour |





| | | | | | | 0.25-20 MHz | film |
|----|------------|-------|-------|-------|----|--|-----------------------|
| 12 | 26-01-1990 | 19:30 | 20:28 | 21:22 | 23 | j3o: C4, cross deltas, 0.25-20 MHz | 1 hour film |
| 13 | 03-11-1994 | 11:49 | 12:45 | 13:46 | 45 | j3o: C4, cross deltas, 0.25-20 MHz | 1 hour film |
| 14 | 11-09-2007 | 11:03 | 11:46 | 12:55 | 49 | j3o: IPS 42, cross deltas, 1-22 MHz | 15 min digital |
| 15 | 11-07-2010 | 19:54 | 20:58 | 21:47 | 62 | j3o: IPS 42, cross deltas, 1-22 MHz | No data |
| 16 | 13-11-2012 | 22:48 | 23:34 | 23:34 | 63 | j3p: IPS 42, cross deltas, 1-22 MHz | 15 min digital |
| 17 | 26-02-2017 | 12:18 | 13:30 | 14:51 | 67 | ј3р | Instrument failure |
| 18 | 02-07-2019 | 19:16 | 20:31 | 21:38 | 81 | ј3р | Instrument failure |
| 19 | 14-12-2020 | 14:36 | 16:00 | 17:28 | 92 | j3p: IPS 42, cross deltas, 1-22 MHz | 1 min digital |
| 20 | 30-04-2022 | 20:21 | 21:30 | 22:03 | 34 | j3p: IPS 42, cross deltas, 1-22 MHz | 15 min digital |
| 21 | 02-10-2024 | 18:56 | 20:24 | 21:42 | 55 | j3p: IPS 42, cross deltas, 1-22 MHz | 15 min digital |
| 22 | 06-02-2027 | 13:21 | 14:56 | 16:39 | 70 | j3p: IPS 42, cross deltas, 1-22 MHz | - |

153 Using the established regression relationships, we computed predicted ionospheric responses for the upcoming 06 February 154 2027 solar eclipse, during which Chillán is expected to experience approximately 70% solar obscuration (last row of Table 155 1). These predictions are indicated by orange star markers in all regression plots, providing quantitative forecasts to support 156 observation campaign planning.

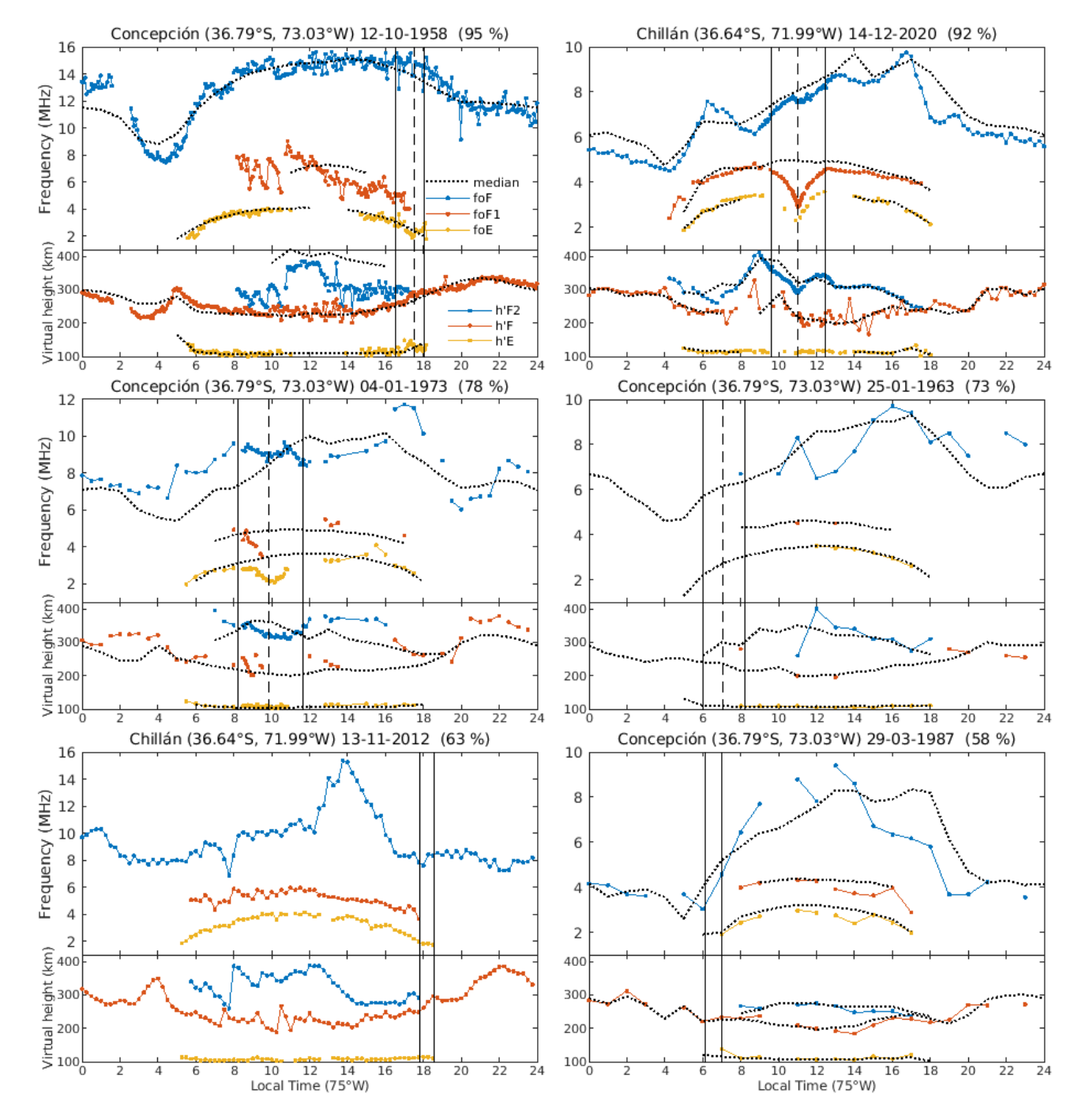
157 3 Results and Discussion

158 The diurnal variations of critical frequencies and virtual heights observed during the days in which the 16 selected eclipses 159 occur are shown in Figures 1 to 3. Diurnal variations of monthly mean values are also shown as reference. As already 160 indicated, observed values are given at different time intervals as appropriate to the available ionograms for the different 161 eclipses. The diurnal variations are arranged according to the darkness level, regardless of the time-of-day, month, year or 162 solar activity epoch.



163



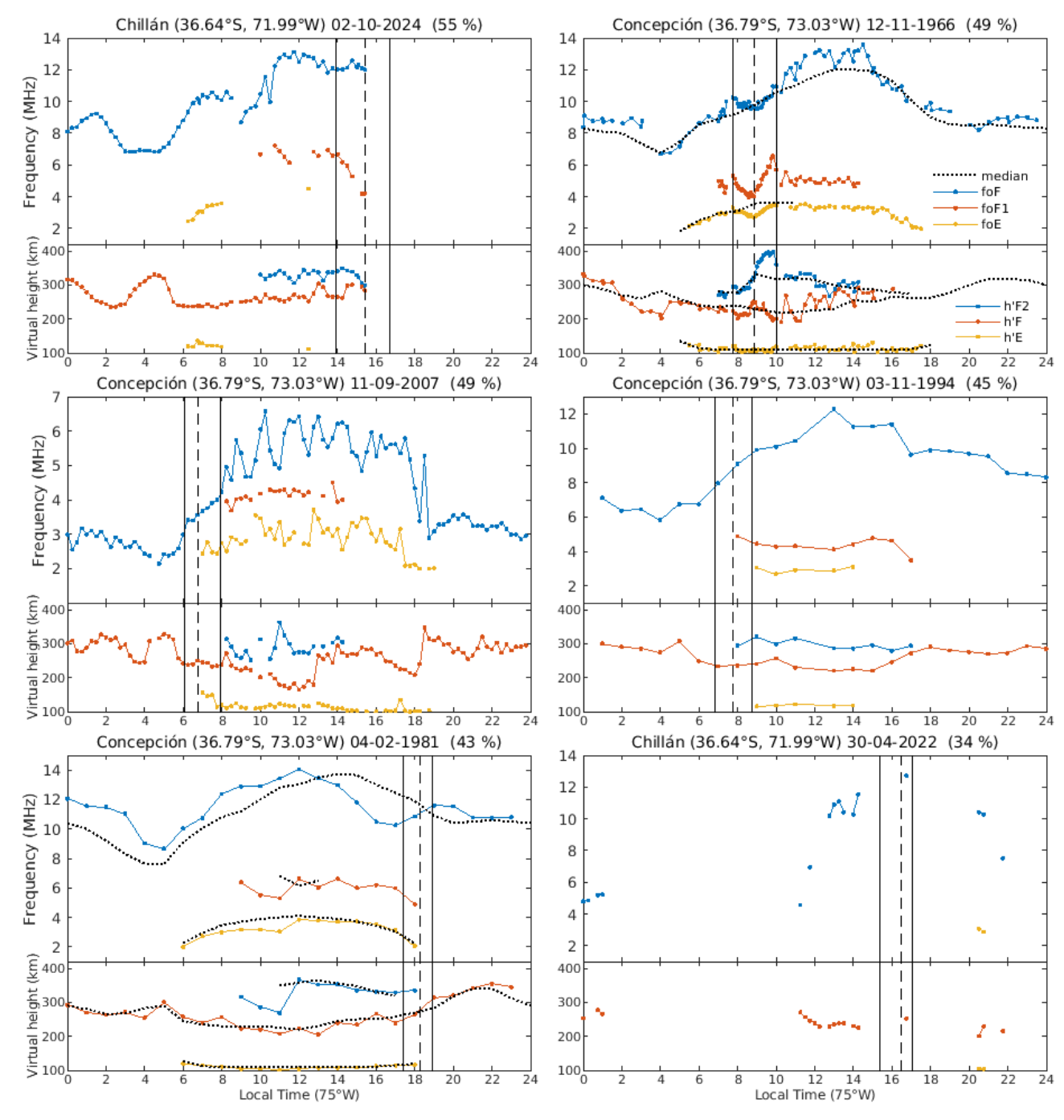


164 Figure 1: Diurnal variation of observed critical frequencies and virtual height (dots) on days of various solar eclipses with 165 darkness level > 55%, and of corresponding monthly median values (dotted line). Continuous vertical line indicates onset and end 166 of eclipse. Slashline indicates the time of maximum darkness.



167

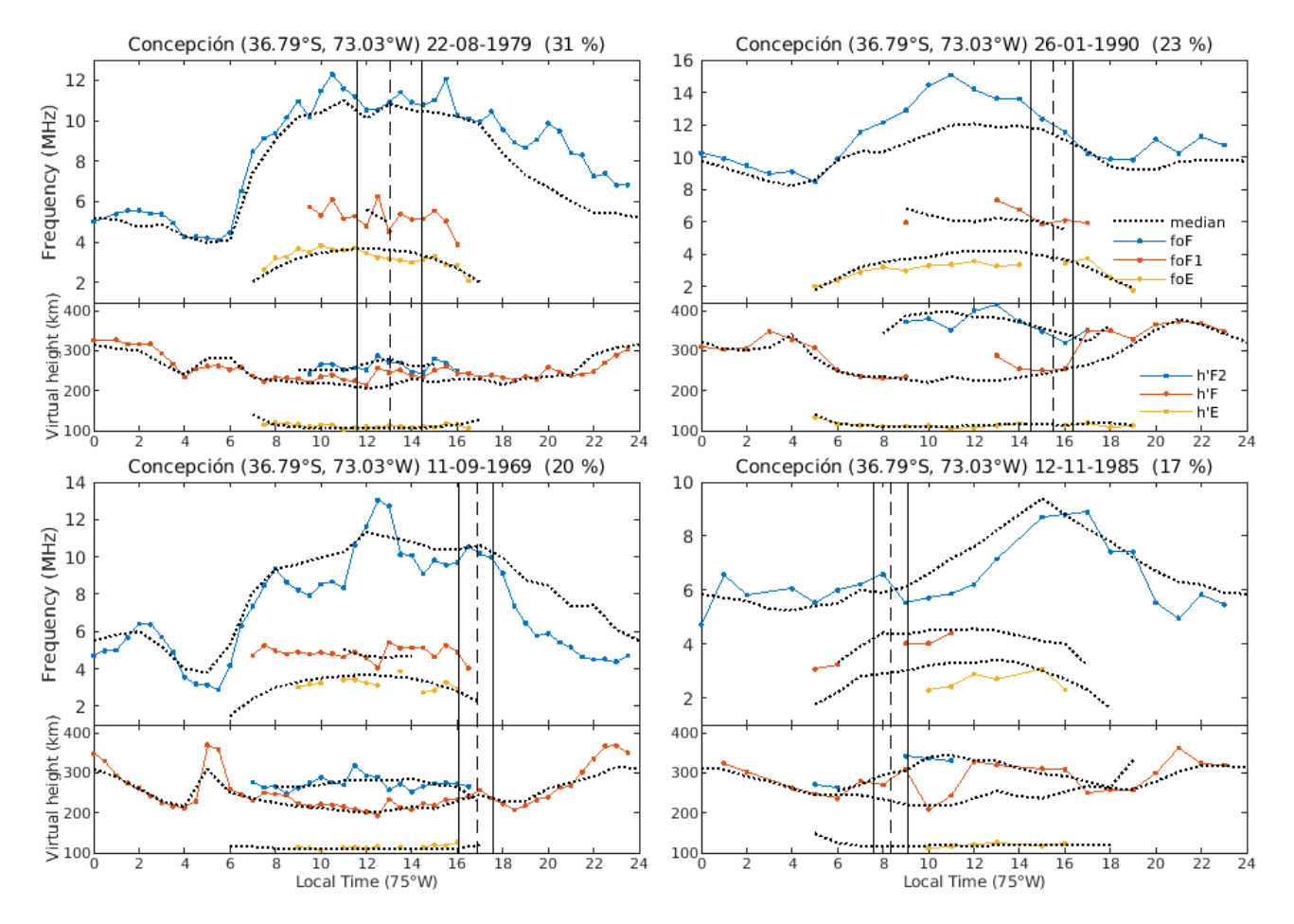




168 Figure 2: As of Figure 1 but for darkness level between 34 % and 55 %.







170 Figure 3: Same as Figure 1, but for darkness level between 17 % and 31 %.

171 As it is obvious, the clearer ionospheric effects of eclipses are seen during eclipses occurring just before or around local 172 noon. The maximum level of darkness ranges from 31% to 92% for these eclipses, thus allowing to determine a fairly 173 dependence of ionospheric effects on darkness level. The critical frequencies of the F1 and E layers show a typical dip 174 variation during the eclipses. While the critical frequency of the F2 layer has more complex variations, probably showing 175 two different stages, before and after the maximum darkness level, somehow following the variations of h'F2/F. The E layer 176 virtual height does not seem to significantly change during these eclipses.

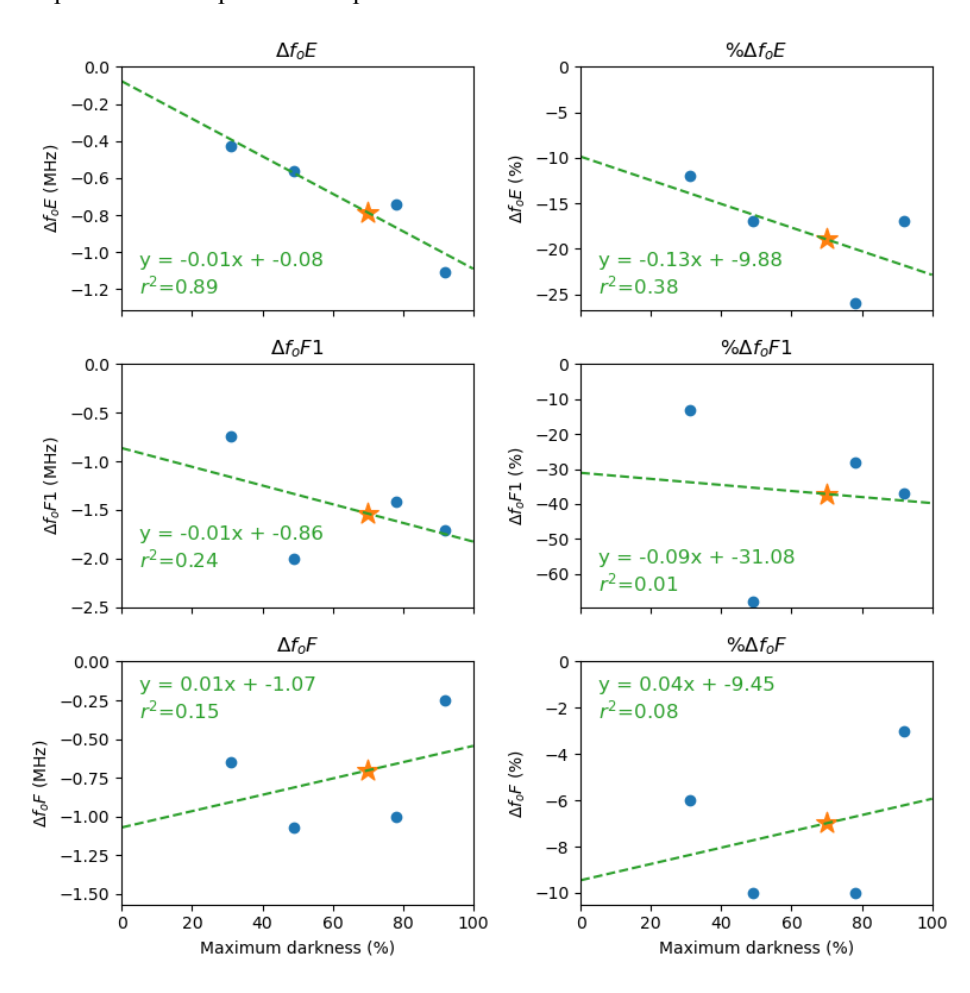
177 It should be noted that the reference curves (dotted lines representing the monthly median hourly values) are shown only for 178 some eclipse events, corresponding to the months for which full-month ionograms had previously been scaled for the World 179 Data Center and for the 2020 eclipse event. For the other cases, reference values for the remaining days of the month were 180 not available.



191



We selected four events exhibiting clear ionospheric signatures and sufficient data coverage during the eclipse period for the regression analysis (Figure 4). The remaining 16 events were not considered due to one or more of the following limitations: (1) missing observations during critical eclipse phases (particularly around maximum obscuration), (2) eclipse occurrence near sunrise or sunset when ionospheric conditions are rapidly changing, making it difficult to isolate eclipse effects from distributions, (3) severe film degradation preventing reliable parameter extraction despite multiple scaling attempts, or obscuration levels below the detection threshold for significant ionospheric perturbations. It should be noted that the regression analysis was performed only on critical frequencies and not on virtual heights. Changes in virtual heights (h'E, h'F1, h'F2/F) were observed to be inconsistent—sometimes increasing, sometimes decreasing—making prediction difficult. These variations are likely influenced by additional factors such as neutral winds, plasma transport, and other dynamical processes, which complicate their response to eclipse conditions.



192 Figure 4: Linear regression analysis of ionospheric parameter deviations versus solar obscuration percentage during four eclipse 193 events (1957–2024, blue circles). Left column: absolute frequency deviations (MHz). Right column: percentage deviations (%). 194 Green dashed lines represent least-squares linear fits with equations and r² values shown. Orange stars indicate predicted 195 responses for the 06 February 2027 eclipse (70% obscuration at Chillán).





196 The E-layer critical frequency (foE) exhibited a robust linear response to solar obscuration, with absolute deviations 197 showing the strongest correlation among all analyzed parameters ($r^2 = 0.89$, n = 4 events, Figure 4, upper left panel). The 198 regression yielded a slope -0.01 of MHz per percent obscuration and an intercept of -0.08 MHz, indicating that foE 199 decreases nearly proportionally to eclipse magnitude. This relationship implies that a hypothetical total eclipse (100% obscuration) would reduce foE by approximately 1.0 MHz relative to unperturbed reference conditions.

201 The high predictive power ($r^2 = 0.89$) reflects the rapid photochemical equilibrium characteristic of the E-region, where 202 recombination timescales (20-40 minutes) are comparable to or shorter than typical eclipse durations. Consequently, E-layer 203 ionization density responds almost instantaneously to variations in solar EUV flux, with minimal influence from dynamic 204 processes such as neutral winds or plasma diffusion that complicate interpretation of higher-altitude layers.

205 When expressed as percentage deviations (% Δ foE, Figure 4, upper right panel), the correlation weakened substantially (r² = 206 0.38), with a regression slope of -0.13 % obscuration. This degradation reflects the additional variability introduced by 207 diurnal, seasonal, and solar cycle variations in baseline foE values, which range from ~2 MHz during solar minimum to >4 208 MHz during solar maximum. A fixed absolute reduction (e.g., 0.7 MHz) thus translates to percentage deviations spanning 209 17-35% depending on background conditions, increasing scatter in the normalized representation.

210 Based on the established relationship, the 06 February 2027 eclipse (70% obscuration at Chillán) is predicted to induce a 211 foE reduction of 0.7 MHz (orange star, Figure 4). This forecast will enable direct validation of the regression model and 212 assessment of its predictive skill across different solar cycle phases.

213 Several campaigns were conducted historically to obtain ionograms at higher temporal resolution during eclipses, with 214 observations every 5 minutes for significant events. However, most of these high-cadence data were never published. For 215 the 2 July 2019 solar eclipse, there was a unique opportunity to measure the ionospheric response at two locations in Chile: 216 Chillán (36.64°S, 71.99°W) and La Serena (29.9°S, 71.3°W). However, the ionosonde in Chillán failed during the event, so 217 only the response at La Serena was published (Bravo et al., 2020). One of the analyzed events corresponds to the 14 218 December 2020 solar eclipse over Chillán, for which ionospheric responses were also studied by de Haro Barbas et al. 219 (2022). Their results included calculations of the alpha and beta recombination coefficients, which were found to be 220 consistent with values reported by previous authors, confirming the reliability of the ionospheric observations in this region. 221 Inclusive, prior to the 2020 eclipse, a prediction of the ionospheric response over the Chillán station had been performed 222 using the SUPIM-INPE model, estimating the expected variations in the different ionospheric layers during the event 223 (Martínez-Ledesma et al., 2020). This prediction was later validated using the observed ionospheric data, as reported in 224 Bravo et al. (2022), showing good agreement between the modeled and measured responses.





225 It is important to highlight the dedicated effort of ionosonde operators and technicians, particularly during the 1958–1994 226 period, who ensured continuous monitoring and undertook the considerable effort of recording frequent ionograms during 227 eclipses.

228 The present study relied on a historical dataset that represents a significant rescue of scientific heritage. Many records were 229 on obsolete 35 mm film, degraded, or even potentially flammable, and have now been digitized and standardized for 230 analysis. Similar conditions exist at other older ionospheric stations, emphasizing the importance of preserving long-term 231 ionospheric observations and fully exploiting their scientific value.

232 4 Conclusion

233 This work analyzed the response of the Concepción/Chillán ionosphere to 16 selected solar eclipses, out of a total of 21 234 identified events over the period 1958–2024, using a long-term historical ionogram dataset. Critical frequencies and virtual 235 heights were extracted from scaled ionograms, and regression analysis was performed to quantify the relationship between 236 solar obscuration and ionospheric parameter deviations. The study demonstrates that the E-layer responds nearly linearly to 237 eclipse-induced reductions in solar radiation, while higher layers, particularly the F2 layer, exhibit more complex and 238 variable behavior due to additional dynamical processes. High-resolution observations, when available, provided insights 239 into short-term responses and enabled predictions for future eclipses.

Regression analysis focused exclusively on critical frequencies, as virtual heights often exhibited inconsistent behavior, reflecting the influence of neutral winds, plasma transport, and other dynamical factors that complicate their interpretation. It is important to note that only the ionospheric responses measured at Chillán during the 2 July 2019 and 14 December 2020 eclipses were published; no data from the remaining eclipse events have been published. The success of this study relied heavily on the dedication of ionosonde operators and technicians, particularly during the 1958–1994 period, who ensured frequent and reliable observations during solar eclipses. Moreover, this work represents a significant rescue of scientific heritage, digitizing and standardizing records that were previously on fragile or potentially hazardous 35 mm film.

248 Predictions for the upcoming 06 February 2027 eclipse, with an expected 70% obscuration at Chillán, indicate a foE 249 decrease of approximately 0.7 MHz, providing a clear opportunity to validate the regression models and assess their 250 predictive skill across different solar cycle conditions.





251 Author contributions

- 252 AYG: writing (original draft preparation) and data curation; MAB: Conceptualization, writing (original draft preparation)
- 253 and formal analysis; CAC-R: data curation; MRC: data curation; BAU: methodology and data curation; AJF: supervision
- 254 and validation.

255

256 Competing interests

257 Manuel Bravo is the guest editor of the special issue.

258

259 Acknowledgements

- 260 We are indebted to the engineers and technicians who operated the C4 and IPSS-42 ionosondes from 1957 onwards; without
- 261 their work, this report would not have been possible. In particular, we thank Carlos Figueroa, Herwing Herrera, José Rivera,
- 262 Avelino Sáez, and others. This work was supported by the Universidad Adventista de Chile, regular projects PI-175 and
- 263 PI-204. MAB and BAU acknowledge the ANID SUBDIRECCIÓN DE INVESTIGACIÓN APLICADA/ID25110556. The
- 264 authors acknowledge the assistance of Sider ai in the translation and preliminary review of the manuscript draft, with the
- 265 subsequent and exhaustive manual scientific validation.

266 References

- 267 Bravo, M. A., Foppiano, A. J., and Abarca del Río, R.: Long-Term Dependencies of Annual and Semiannual Components of
- 268 NmF2 Over Concepción. The Open Atmospheric Science Journal, 5(1), 2-8, doi: 10.2174/1874282301105010002, 2011.
- 269 Bravo, M., Martínez-Ledesma, M., Foppiano, A., Urra, B., Ovalle, E., Villalobos, C., Souza, J., Carrasco, E., Muñoz, P.,
- 270 Tamblay, L., Vega-Jorquera, P., Marín, J., Pacheco, R., Rojo, E., Leiva, R. & Stepanova, M.: First report of an eclipse from
- 271 Chilean ionosonde observations: comparison with total electron content estimations and the modeled maximum electron
- 272 concentration and its height. J. Geophys. Res. Space Physics, 125, e2020JA027923. doi:10.1029/2020JA027923, 2020.
- 273 Bravo M.A., Molina M.G., Martínez-Ledesma M., de Haro Barbás B., Urra B., Elías A., Souza J., Villalobos C., Namour
- 274 J.H., Ovalle E., Venchiarutti J.V., Blunier S., Valdés-Abreu J.C., Guillermo E., Rojo E., de Pasquale L., Carrasco E., Leiva
- 275 R., Castillo Rivera C., Foppiano A., Milla M., Muñoz P.R., Stepanova M., Valdivia J.A. and Cabrera M.: Ionospheric
- 276 response modeling under eclipse conditions: Evaluation of 14 December 2020, total solar eclipse prediction over the South
- 277 American sector. Front. Astron Space Sci, 9, doi: 10.3389/fspas.2022.1021910, 2022.
- 278 Bremer, J.: Ionospheric trends in mid-latitudes as a possible indicator of the atmospheric greenhouse effect, Journal of
- 279 Atmospheric and Terrestrial Physics 54, 1505-1511, 1992.
- 280 Chuo, Y. J.: Ionospheric effects on the F region during the sunrise for the annular solar eclipse over Taiwan on 21 May
- 281 2012, Ann. Geophys., 31, 1891–1898, doi:10.5194/angeo-31-1891-2013, 2013.





- 282 de Haro Barbás, BF, Bravo, M, Elias, AG, Martínez-Ledesma, M, Molina, G, Urra, B, Venchiarutti, JV, Villalobos, C,
- 283 Namour, JH, Ovalle, E, Guillermo, ED, Carrasco, E, de Pasquale, G, Rojo, E, Leiva R. Longitudinal variations of
- 284 ionospheric parameters near totality during the eclipse of December 14, 2020. Adv. Space Res.,
- 285 doi:10.1016/j.asr.2021.12.026, 2022.
- 286 Foppiano, A.J.; Cid, L. and Jara, V.:, Ionospheric long-term trends in South American mid-latitudes, Journal of Atmospheric
- 287 and Solar-Terrestrial Physics, 61, 717-723, 1999.
- 288 Hoque M.M., Wenzel, D., Jakowski, N., Gerzen, T., Berdermann, J., et al.: Ionospheric response over Europe during the
- 289 solar eclipse of March 20, 2015. J. Space Weather Space Clim., 6, A36, doi:10.1051/swsc/2016032, 2016.
- 290 Jarvis, M.J., Jenkins, B., Rodgers, G.A.: Southern hemisphere observations of long-term decrease in F-region altitude and
- 291 thermospheric wind providing possible evidence for global thermospheric cooling, Journal of Geophysical Research, 103,
- **292** 20774-20787, 1998.
- 293 Lastovicka, J.: Progress in investigating long-term trends in the mesosphere, thermosphere, and ionosphere, Atmos. Chem.
- 294 Phys., 23, 5783-5800, doi:10.5194/acp-23-5783-2023, 2023.
- 295 Laštovi cka, J., Solomon, S.C. and Qian, L.: Trends in the Neutral and Ionized Upper Atmosphere, Space Sci Rev,
- 296 doi:10.1007/s11214-011-9799-3, 2017.
- 297 Le, H., Liu, L., Yue, X., and Wan, W.: The ionospheric responses to the 11 August 1999 solar eclipse: observations and
- 298 modeling, Ann. Geophys., 26, 107–116, doi:10.5194/angeo-26-107-2008, 2008.
- 299 Le, H., Liu, L., Yue, X., Wan, W., and Ning B.: Latitudinal dependence of the ionospheric response to solar eclipses,
- 300 J. Geophys. Res., 114, A07308, doi:10.1029/2009JA014072, 2009.
- 301 Martínez-Ledesma, M., Bravo, M., Urra, B., Souza, J., and Foppiano, A.: Prediction of the ionospheric response to the 14
- 302 December 2020 total solar eclipse using SUPIM-INPE. JGR. Space Phys. 125, e2020JA028625.
- 303 doi:10.1029/2020JA028625, 2020.
- 304 Masana, E.: Eclipsi 2.0 (Eclipse Calculator 2.0) [Mobile application software]. ServiAstro Universitat de Barcelona.
- 305 Available in: https://serviastro.ub.edu/en/materials/apps/eclipsi-20, 2012.
- 306 Muzzioli, L.: La Estación de la Ionósfera, Atenea No. 435, 1er Semestre, 179-191, 1977.
- 307 Ortiz de Adler, N., Elías, A.G., Manzano, J.R.: Solar cycle length variations: its relation with ionospheric parameters.
- 308 Journal of Atmospheric and Terrestrial Physics 59, 159-162, 1997.
- 309 Ovalle E. M., Villalobos C. U., Agüero L. A., Leiva R. E., Foppiano A. J.: A new ionospheric station for Chile, Bulletin No
- 310 74, Ionospheric Network Advisory Group, Union Radio Scientific Internationale, 2017.
- 311 Ramíırez, P.M.: Física de la ionósfera e interpretación de los ionogramas obtenidos en la Estación Concepción, como
- 312 colaboración al Año Geofísico Internacional, Facultad de Ingeniería, Universidad de Concepción, 1963.
- 313 Ratcliffe, J. A.: A survey of solar eclipses and the ionosphere. In W. J. G. Beynon & G. M. Brown (Eds.), Solar eclipses and
- 314 the ionosphere (pp. 1–13). Oxford: Pergamon Press, 1956.





- 315 Smith, P.A., King, J.W.: Long-term relationships between sunspots, solar faculae and the ionosphere. Journal of
- 316 Atmospheric and Terrestrial Physics 43, 1057-1063, 1981.
- 317 Zhang, H., Zhang, T., Zhang, X., Yuan, Y., Wang, Y., & Ma, Y.: Multi-Instrument Observations of the Ionospheric Response
- 318 Caused by the 8 April 2024 Total Solar Eclipse. Remote Sensing, 16(13), 2451, doi:10.3390/rs16132451, 2024.